

## MIT Open Access Articles

*Epitaxial growth of large-area and highly crystalline anisotropic ReSe<sub>2</sub> atomic layer*

The MIT Faculty has made this article openly available. **Please share** how this access benefits you. Your story matters.

**Citation:** Cui, Fangfang et al. "Epitaxial growth of large-area and highly crystalline anisotropic ReSe<sub>2</sub> atomic layer." Nano Research 10, 8 (August 2017): 2732-2742 © 2017 Tsinghua University Press and Springer-Verlag Berlin Heidelberg

**As Published:** <http://dx.doi.org/10.1007/s12274-017-1477-7>

**Publisher:** Springer Nature

**Persistent URL:** <https://hdl.handle.net/1721.1/121436>

**Version:** Author's final manuscript: final author's manuscript post peer review, without publisher's formatting or copy editing

**Terms of use:** Creative Commons Attribution-Noncommercial-Share Alike



# Epitaxial growth of large-area and highly crystalline anisotropic ReSe<sub>2</sub> atomic layer

Fangfang Cui<sup>1</sup>, Xiaobo Li<sup>1</sup>, Qingliang Feng<sup>2</sup>, Jianbo Yin<sup>2</sup>, Lin Zhou<sup>3</sup>, Dongyan Liu<sup>1</sup>, Kaiqiang Liu<sup>1,4</sup>, Xuexia He<sup>1</sup>, Xing Liang<sup>1</sup>, Shengzhong Liu<sup>1</sup>, Zhibin Lei<sup>1</sup>, Zonghuai Liu<sup>1</sup>, Hailin Peng<sup>2</sup>, Jin Zhang<sup>2</sup>, Jing Kong<sup>3</sup>, and Hua Xu<sup>1</sup> (✉)

<sup>1</sup>Key Laboratory of Applied Surface and Colloid Chemistry, Ministry of Education, Shaanxi Key Laboratory for Advanced Energy Devices; Shaanxi Engineering Lab for Advanced Energy Technology, School of Materials Science and Engineering, Shaanxi Normal University, Xi'an 710119, China

<sup>2</sup>Center for Nanochemistry, Beijing National Laboratory for Molecular Sciences, Key Laboratory for the Physics and Chemistry of Nanodevices, College of Chemistry and Molecular Engineering, Peking University, Beijing 100871, China

<sup>3</sup>Department of Electrical Engineering and Computer Sciences, Massachusetts Institute of Technology, Cambridge, MA 02139, USA

<sup>4</sup>School of Chemistry and Chemical Engineering, Shaanxi Normal University, Xi'an 710119, China

**Received:** 24 November 2016

**Revised:** 29 December 2016

**Accepted:** 5 January 2017

© Tsinghua University Press and Springer-Verlag Berlin Heidelberg 2017

## KEYWORDS

rhodium diselenide (ReSe<sub>2</sub>), epitaxial growth, high crystal quality, anisotropy, optoelectronics

## ABSTRACT

The anisotropic two-dimensional (2D) layered material rhenium disulfide (ReSe<sub>2</sub>) has attracted considerable attention because of its unusual properties and promising applications in electronic and optoelectronic devices. However, because of its low lattice symmetry and interlayer decoupling, anisotropic growth and out-of-plane growth occur easily, yielding thick flakes, dendritic structure, or flower-like structure. In this study, we demonstrated a bottom-up method for the controlled and scalable synthesis of ReSe<sub>2</sub> by van der Waals epitaxy. To achieve controllable growth, a micro-reactor with a confined reaction space was constructed by stacking two mica substrates in the chemical vapor deposition system. Within the confined reaction space, the nucleation density and growth rate of ReSe<sub>2</sub> were significantly reduced, favoring the large-area synthesis of ReSe<sub>2</sub> with a uniform monolayer thickness. The morphological evolution of ReSe<sub>2</sub> with growth temperature indicated that the anisotropic growth was suppressed at a low growth temperature (<600 °C). Field-effect transistors employing the grown ReSe<sub>2</sub> exhibited p-type conduction with a current ON/OFF ratio up to 10<sup>5</sup> and a hole carrier mobility of 0.98 cm<sup>2</sup>/(V·s). Furthermore, the ReSe<sub>2</sub> device exhibited an outstanding photoresponse to near-infrared light, with responsivity up to 8.4 and 5.1 A/W for 850- and 940-nm light, respectively. This work not only promotes the large-scale application of ReSe<sub>2</sub> in high-performance electronic devices but also clarifies the growth mechanism of low-lattice symmetry 2D materials.

Address correspondence to xuhua-nano@snnu.edu.cn

## 1 Introduction

Recently, Re-based dichalcogenide materials of the form  $\text{ReX}_2$  ( $X = \text{S}, \text{Se}$ ), which are relatively unexplored transition-metal dichalcogenides (TMDs), have attracted considerable attention because of their unique structure and properties [1–5].  $\text{ReX}_2$  materials, such as rhenium disulfide ( $\text{ReS}_2$ ) and rhenium diselenide ( $\text{ReSe}_2$ ), have a distorted octahedral (1T) crystal structure, resulting from the stabilization of the extra valence electron in each Re atom [6]. The Re atoms within a monolayer form clusters of four Re atoms and interlink in diamond-shaped (DS) chains, yielding considerable anisotropy in the electrical and optical properties [2, 7, 8]. The superior anisotropic properties of  $\text{ReX}_2$  materials, which are similar to those of black phosphorus, endow them with great potential in novel electronic devices [9–13]. Furthermore, unlike  $\text{WS}_2$  and  $\text{MoS}_2$ , the  $\text{ReX}_2$  layers are charge-decoupled from each other because of the Peierls distortion in the 1T structure of  $\text{ReX}_2$ , preventing ordered stacking and minimizing the interlayer overlap of the wave functions [1]. Recently, few-layer  $\text{ReX}_2$  sheets, which exhibit distinct optical and electrical behaviors from group VI TMDs, have been demonstrated as field-effect transistors (FETs), digital inverters, and photodetectors [9, 14–20].

In particular, the narrow bandgap (1.29 eV) and p-type conduction features of  $\text{ReSe}_2$ , which are rare in most TMDs, are highly desired for electronic and optoelectronic devices. However, to date, most fundamental investigations of  $\text{ReSe}_2$  have been largely based on mechanically exfoliated layers synthesized via complex chemical vapor transport [9, 21]. Unfortunately, this method does not allow the controllable and high-throughput manufacturing of two-dimensional (2D) materials. The scalable and controllable deposition of large-area  $\text{ReSe}_2$  atomic layers is essential for further research and applications. Chemical vapor deposition (CVD) is an efficient approach for the scalable synthesis of high-quality 2D TMDs [22–24]. However, owing to its unusual structure and properties,  $\text{ReSe}_2$  is more difficult to fabricate than traditional TMDs such as  $\text{MoS}_2$  and  $\text{WS}_2$ . For example, the distorted 1T structure and the weaker interlayer coupling of  $\text{ReX}_2$  can easily cause anisotropic growth and out-of-plane growth; thus, thick-flake, dendritic, and flower-like structures

have been largely observed for CVD-synthesized  $\text{ReS}_2$  [4, 25, 26]. In the case of 2D  $\text{ReSe}_2$ , the lower chemical reactivity of Se makes it difficult to synthesize; hence, its preparation has been rare. Recently, Zhai et al. for the first time fabricated  $\text{ReSe}_2$  using CVD [27], growing highly crystalline  $\text{ReSe}_2$  flakes on a  $\text{SiO}_2/\text{Si}$  substrate. This was a pioneering work in the synthesis of  $\text{ReSe}_2$ . Currently, the domain size, thickness, and morphology of the  $\text{ReSe}_2$  are uncontrollable. Moreover, our understanding of the mechanisms underlying the unusual behavior and the low lattice symmetry of  $\text{ReSe}_2$  is lacking, which is important for its controlled growth.

In this study, we demonstrated an effective bottom-up method for the controlled and scalable synthesis of large-area, high-quality  $\text{ReSe}_2$  film with uniform monolayer thickness via van der Waals epitaxy. Volatile rhenium trioxide ( $\text{ReO}_3$ ) was used as Re precursor to ensure the growth efficiency, and mica with a low surface energy was used as the substrate to realize the epitaxy growth. To achieve controllable growth, a micro-reactor was constructed by stacking two mica substrates in the CVD system, which reduced the nucleation density and growth rate of  $\text{ReSe}_2$ . Additionally, the weak van der Waals interaction between the atomic flat surface of mica and the adatoms ( $\text{ReSe}_2$  cluster) favored the epitaxial growth. The synergy of the confined reaction space with the epitaxial growth contributed to the large-area synthesis of low-lattice symmetry  $\text{ReSe}_2$  with uniform monolayer thickness. Furthermore, the nucleation density of the  $\text{ReSe}_2$  was modulated by introducing moderate amounts of  $\text{H}_2$  as a carrier gas, which not only controlled the vapor pressure of the Re source through modulation of its valence state but also enhanced the low chemical reactivity of Se. The morphological evolution of  $\text{ReSe}_2$  with respect to the growth temperature suggested that the anisotropic growth was suppressed at a low growth temperature (<600 °C). Angle-resolved polarized Raman spectroscopy indicated the superior optical anisotropic properties of the grown  $\text{ReSe}_2$ . FETs employing the grown monolayer  $\text{ReSe}_2$  exhibited p-type conduction with a current ON/OFF ratio up to  $10^5$  and a hole carrier mobility of  $0.98 \text{ cm}^2/(\text{V}\cdot\text{s})$ , measured under ambient conditions. Moreover, the  $\text{ReSe}_2$  device exhibited an outstanding photoresponse

to near-infrared (NIR) light, with responsivity up to 8.4 and 5.1 A/W for 850- and 940-nm light, respectively. Because of its high crystallinity, superior anisotropy, and controllable growth, ReSe<sub>2</sub> has great potential for applications in future electronic, optoelectronic, and new-concept devices.

## 2 Results and discussion

To synthesize the monolayer ReSe<sub>2</sub> film, ReO<sub>3</sub> and Se powder were introduced as Re and Se precursors, respectively, in a single-zone furnace, as schematically shown in Fig. 1(a). A mixture of Ar (80 sccm) and H<sub>2</sub> (1 sccm) was used as the carrier gas. The typical growth temperature and growth time were 600 °C and 3 min, respectively. ReO<sub>3</sub> is a far better Re precursor for growing ReSe<sub>2</sub> than metal Re (high melting point of 3,180 °C) and NH<sub>4</sub>ReO<sub>4</sub> (yields a low crystal quality)—which were previously used for growing ReS<sub>2</sub> [25, 28]—and can ensure a high growth efficiency and

high crystal quality with a low growth temperature. However, using ReO<sub>3</sub> as Re precursor to grow ReSe<sub>2</sub> introduces a serious problem. When the temperature is increased above 400 °C, the ReO<sub>3</sub> begins to decompose into Re<sub>2</sub>O<sub>7</sub> (sublimes easily) and ReO<sub>2</sub> (less volatile) through the following disproportionation reaction, as shown in Fig. S1 in the Electronic Supplementary Material (ESM).



The extremely high volatility of Re<sub>2</sub>O<sub>7</sub> (melting point of 220 °C and boiling point of 360 °C) yields superabundant nucleation sites during the growth process, causing the growth of a thick film composed of dense ReSe<sub>2</sub> dots on the substrate (Fig. 1(b)). To solve this problem, two pieces of freshly exfoliated mica were tightly stacked, forming a confined reaction space, and then placed above the ceramic boat (see details in Experimental section). We defined the inside surface of the mica as the A face and the top and

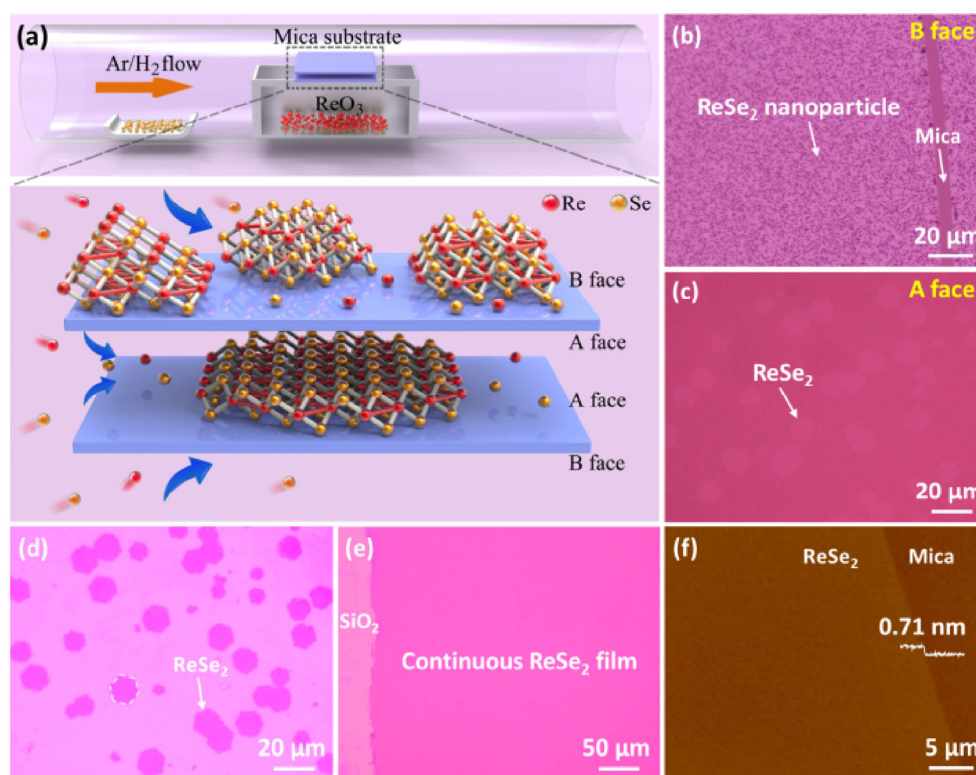


**Figure 1** (a) Schematic of the CVD growth of ReSe<sub>2</sub> in the confined reaction space and the surface reaction during the epitaxial growth of the ReSe<sub>2</sub> atomic layer on mica. Optical microscopy (OM) images of ReSe<sub>2</sub> grown on (b) the B face and (c) the A face of a mica substrate. (d) and (e) Optical images of ReSe<sub>2</sub> grown on the A face, after it was transferred onto a SiO<sub>2</sub>/Si (300 nm) substrate. (f) AFM image of the as-grown ReSe<sub>2</sub> on a mica substrate.

bottom surfaces, which were exposed to the outside, as the B face. The ReSe<sub>2</sub> grown on the B face (Fig. 1(b)) and A face (Fig. 1(c)) of the mica substrate exhibited obvious differences.

As shown in Fig. 1(a), when two pieces of mica were joined tightly, the small crevice between the two mica substrates functioned as a micro-reactor for the growth of ReSe<sub>2</sub>. The micro-reactor played a space-confinement role, decreasing the concentration of precursors and thus decreasing the nucleation density and growth rate of ReSe<sub>2</sub>. As a result, a large-scale ReSe<sub>2</sub> film with domain size up to 20 μm grew on the A faces (Fig. 1(c)), and a continuous monolayer ReSe<sub>2</sub> film was synthesized (Fig. 1(e) and Fig. S2 (in the ESM)) when the growth time was extended to 10 min. Atomic force microscopy (AFM) revealed that the grown ReSe<sub>2</sub> film had a thickness of ~0.71 nm, demonstrating a uniform monolayer [21]. When several pieces of mica were stacked together to form a multilayer-sandwich structure as the growth substrate, a uniform monolayer ReSe<sub>2</sub> film grew on the A face of each piece of mica, indicating the scalable growth of the ReSe<sub>2</sub> film.

We also synthesized ReSe<sub>2</sub> on a SiO<sub>2</sub>/Si substrate using the same approach but obtained only flower-like structures (indicating out-of-plane growth) or thick flakes grown on the substrate, as shown in Fig. S3 in the ESM. These are typical features of low-lattice symmetry 2D materials (such as ReS<sub>2</sub>), according to recent studies [4, 25, 26]. The obvious differences in the thickness and morphology between products grown on mica and those grown on SiO<sub>2</sub> substrates are attributed to the variation of the migration barrier energy ( $E_m$ ) and the substrate–adatom interaction. The  $E_m$  of adatoms on SiO<sub>2</sub> surface is far larger than that on mica because of the stronger interaction between the adatoms and the SiO<sub>2</sub> substrate, which has numerous unsaturated dangling bonds [29]. The migration coefficient  $D$  is related to  $E_m$  as follows

$$D \propto e^{-E_m/kT} \quad (2)$$

where  $k$  is the Boltzmann constant, and  $T$  is the substrate temperature [29]. The migration coefficient for the SiO<sub>2</sub> surface is far lower than that for mica with the same growth temperature and time. Hence, the atomically flat surface of mica facilitated precursor

migration during the CVD growth, improving the thickness uniformity of the resulting ReSe<sub>2</sub> layer. Additionally, the weak van der Waals interaction between the mica surface and the ReSe<sub>2</sub> clusters plays a surface-confinement role during the growth process [29, 30], which can efficiently suppress the out-of-plane growth (see detail discussion in S3 in the ESM). Therefore, the combination of space-confined and surface-confined CVD growth is crucial for the controlled fabrication of low-lattice symmetry ReSe<sub>2</sub> materials.

The Raman spectra of as-grown monolayer, bi-layer, tri-layer, and bulk ReSe<sub>2</sub> samples were collected using a 532-nm excitation laser (Fig. 2(a)). A series of Raman modes occupied the frequency range of 100 to 300 cm<sup>-1</sup>, which well matches the spectra for mechanically exfoliated ReSe<sub>2</sub> samples [10, 21]. The characteristic Raman peak at 125 cm<sup>-1</sup> corresponds to an E<sub>g</sub>-like mode, and the peaks at 160 and 174 cm<sup>-1</sup> correspond to A<sub>g</sub>-like modes. Notably, the Raman spectra show a slightly sensitivity to the layer number because of the interlayer decoupling of the ReSe<sub>2</sub> [21, 31]. Photoluminescence (PL) measurements were performed to determine the bandgap of the grown ReSe<sub>2</sub> film (Fig. 2(b)). From bulk to monolayer ReSe<sub>2</sub>, the energy position of the PL shifted slightly from 1.29 to 1.31 eV, indicating that the bandgap of ReSe<sub>2</sub> increased as the number of layers decreased. This is because thinning the flake did not enhance the quantum confinement of the electrons in the system, and neighboring monolayers in the flake were largely electronically decoupled [1, 10]. Additionally, owing to the indirect-bandgap nature of ReSe<sub>2</sub>, the peak intensity was relatively weak for the monolayer ReSe<sub>2</sub> and increased monotonically as layers increasing [10]. These spectral features of the CVD-grown ReSe<sub>2</sub> exhibit stark contrast to the typical behavior of Mo- and W-based TMDs, where the PL intensity of the monolayer is enhanced by orders of magnitude as a result of the crossover from the indirect bandgap in the bulk material to the direct bandgap in monolayers [32]. Furthermore, the CVD-grown ReSe<sub>2</sub> had strong optical anisotropic properties, as indicated by the angle-resolved polarized Raman spectra (see below). Owing to its narrow bandgap and unusual anisotropy, ReSe<sub>2</sub> has great potential for application in future



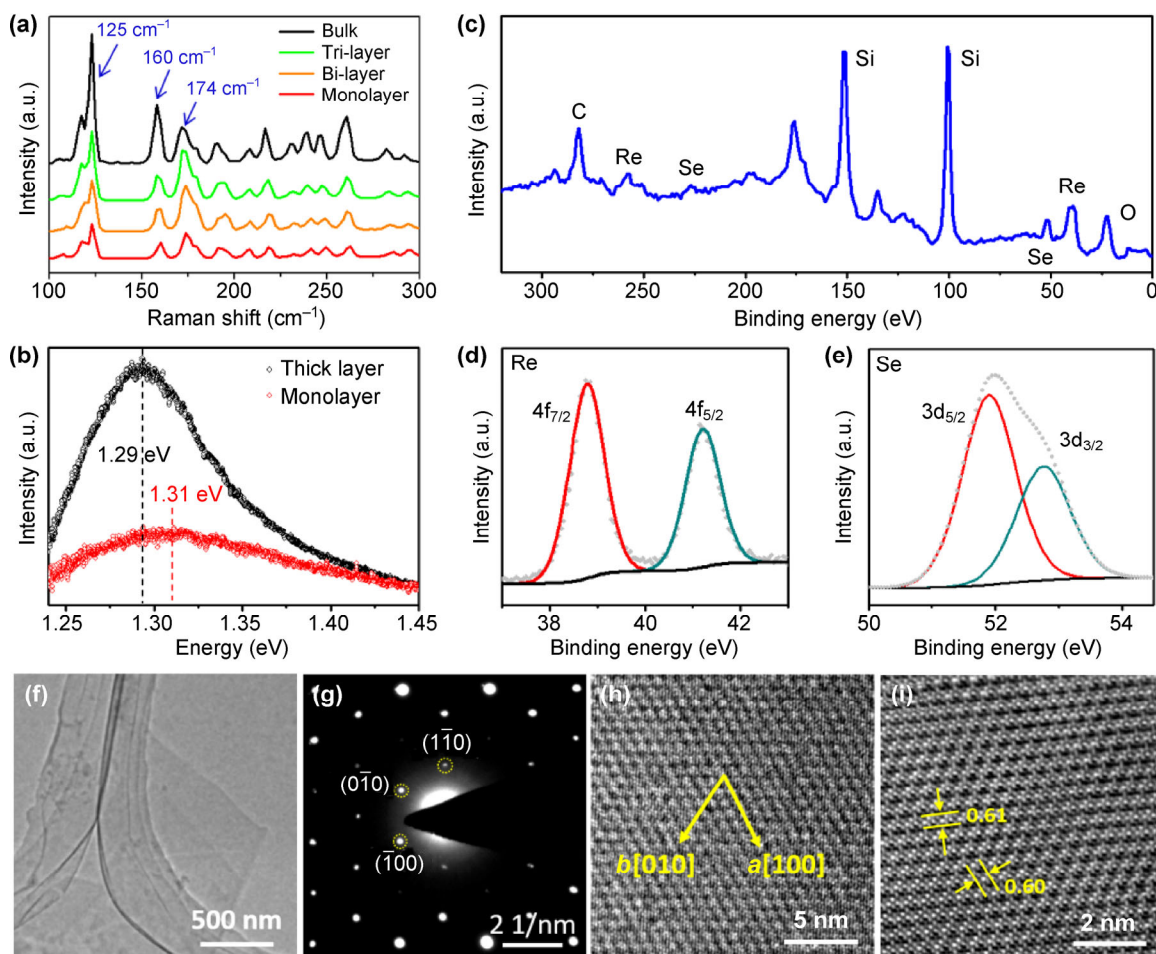


**Figure 2** Characterization of the composition and structure of the CVD-grown ReSe<sub>2</sub> film. (a) Raman and (b) fluorescence spectra of as-grown ReSe<sub>2</sub> with different numbers of layers (excitation wavelength 532 nm). (c) Full XPS spectra of the grown ReSe<sub>2</sub> sample. (d) and (e) Detailed XPS signals of the Re 4f and Se 3d spectra, respectively. (f) Low-resolution TEM image of the ReSe<sub>2</sub> supported on a TEM grid. (g) SAED patterns and (h) HRTEM image of the ReSe<sub>2</sub>. (i) Fast Fourier transform-filtered image of the ReSe<sub>2</sub> shown in (h).

optoelectronic devices, such as photodetectors for NIR or polarized light.

X-ray photoemission spectroscopy (XPS) was performed to confirm the elemental composition and bonding of the grown ReSe<sub>2</sub> samples. Five elements are represented in the spectra (Fig. 2(c)): the signals of Re and Se come from the ReSe<sub>2</sub> samples, those of Si and O come from SiO<sub>2</sub> substrate, and that of C comes from the poly(methyl methacrylate) (PMMA) residue generated during the wet transfer process. Detailed information regarding the Re and Se signals is presented in Figs. 2(d) and 2(e), respectively. The core-level peaks corresponding to the Re 4f<sub>7/2</sub> and 4f<sub>5/2</sub> are located at ~38.8 and ~41.2 eV, respectively. The Se 3d peak around 52.0 eV can be divided into Se 3d<sub>5/2</sub>

and Se 3d<sub>3/2</sub>, which have peak positions of ~51.9 and ~52.8 eV, respectively. These features are consistent with the XPS spectra for the ReSe<sub>2</sub> bulk crystal. Additionally, the ratio of nearly 1:2 of Re to Se suggests that the CVD-grown ReSe<sub>2</sub> was reasonably stoichiometric.

To further analyze the crystallographic structure of the grown ReSe<sub>2</sub>, we performed high-resolution transmission electron microscopy (HRTEM) and selected-area electron diffraction (SAED) by transferring ReSe<sub>2</sub> onto a TEM grid. Figure 2(f) shows a low-magnification TEM image of the ReSe<sub>2</sub> film, in which a clean and uniform membrane is observed. The SAED patterns clearly resolve the *a*[100] and *b*[1 $\bar{1}$ 0] orientations of the distorted 1T crystal, suggesting that

our ReSe<sub>2</sub> is of high quality (Fig. 2(g)). The HRTEM image in Fig. 2(h) shows a clear lattice fringe with interplanar distances of 0.61 and 0.60 nm between the two vicinal DS chains in the directions of *b* and *a* (Fig. 2(i)), respectively.

Usually, the lower chemical reactivity of Se makes Se-based TMDs more difficult to synthesize than S-based TMDs [26]. Moreover, as previously illustrated, the ReO<sub>3</sub> tends to be disproportionate to the volatile Re<sub>2</sub>O<sub>7</sub>, which complicates the synthesis of ReSe<sub>2</sub>. We improved and modulated the growth of the ReSe<sub>2</sub> crystals by tuning the H<sub>2</sub> content in the carrier gas (Fig. 3). When ReSe<sub>2</sub> was grown without H<sub>2</sub>, the oversaturated Re<sub>2</sub>O<sub>7</sub> vapor in the reactor caused an excessive growth rate, leading to large, thick flakes (Fig. 3(a)). In contrast, when a small amount of H<sub>2</sub> (1 sccm) was introduced into the growth system, a monolayer ReSe<sub>2</sub> film was obtained (Fig. 3(b)) owing to the reduction of the volatile Re<sub>2</sub>O<sub>7</sub> into the lower-valence state ReO<sub>3-x</sub>. On the other hand, H<sub>2</sub> can enhance the chemical reactivity of Se by reducing it into H<sub>2</sub>Se [33–36]. As a result, the nucleation density of the ReSe<sub>2</sub> increased significantly with the increase of the H<sub>2</sub> content (Figs. 3(b)–3(d)). Of course, excessive H<sub>2</sub> (>10 sccm) decreased the growth efficiency of the ReSe<sub>2</sub>

because the volatile Re<sub>2</sub>O<sub>7</sub> was completely reduced into less-volatile ReO<sub>2</sub> or Re, as shown in Fig. S4 in the ESM. Therefore, introducing an appropriate amount of H<sub>2</sub> is important for controlling the thickness and nucleation density of ReSe<sub>2</sub>.

Notably, the morphology of ReSe<sub>2</sub> differed significantly according to the growth temperature, changing from a regular hexagon at low temperatures to an irregular dendritic shape at high temperatures (Figs. 3(e)–3(h)). The dendritic morphology of the ReSe<sub>2</sub> indicates the anisotropic growth, which is a typical growth feature of low-lattice symmetry 2D materials and is attributed to the anisotropic interfacial energy induced by the distorted 1T structure [28]. The temperature-modulated morphological evolution is explained by the temperature-dependent migration coefficient of the adatoms on the substrate (see Eq. (2)) [37]. At high growth temperatures, the large migration energy of the adatoms caused them to freely diffuse on the surface of the substrate, and they tended to attach to the ReSe<sub>2</sub> edge (or crystal axis) with a favorable energy. In this case, the fast atomic diffusion apparently caused the anisotropic growth, yielding the irregular dendritic morphology of the ReSe<sub>2</sub>. In contrast, at low growth temperatures, because of the

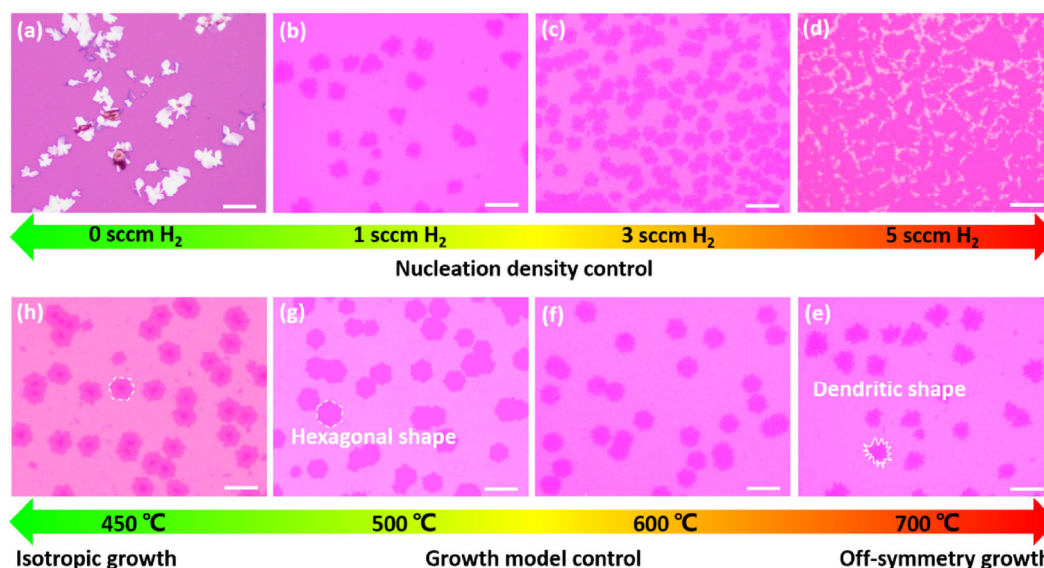


**Figure 3** Control of the nucleation density and morphology of ReSe<sub>2</sub> by modulating the H<sub>2</sub> concentration and growth temperature. (a)–(d) OM images of the ReSe<sub>2</sub> film grown using the mixture of Ar (80 sccm) and H<sub>2</sub> as a carrier gas with H<sub>2</sub> flow rates of (a) 0, (b) 1, (c) 3, and (d) 5 sccm. (e)–(h) OM images of ReSe<sub>2</sub> grown at (e) 700, (f) 600, (g) 500, and (h) 450 °C, at an H<sub>2</sub> flow rate of 1 sccm. All of these OM images were measured for samples transferred from mica onto SiO<sub>2</sub>/Si (300 nm). The scale bar represents 20 μm. The growth time was 3 min for all of these experiments.

slow atomic diffusion and the inhibited attachment and detachment of the adatoms at the ReSe<sub>2</sub> edges, the ReSe<sub>2</sub> grew at different edges with nearly the same rate; thus, the anisotropic growth was suppressed. Our results indicate that the anisotropic growth of ReSe<sub>2</sub> was significantly reduced at low temperatures (<600 °C), yielding materials with a regular morphology. Recent studies on the growth of Re-based TMDs showed that there are sub-domains in its crystal structure and that the Re chain direction changes from one sub-domain to another [7, 27, 38]. According to these studies, the hexagon ReSe<sub>2</sub> domain should be composed of six sub-domains, which is similar to that of recently reported CVD-grown ReS<sub>2</sub> [38]. Furthermore, the Raman spectra of ReSe<sub>2</sub> grown at different temperatures indicate that high-quality ReSe<sub>2</sub> was obtained over the entire temperature range, as shown in Fig. S5 in the ESM. Therefore, the growth temperature played an important role in controlling the morphology of ReSe<sub>2</sub>.

For revealing the optical anisotropy of the CVD-grown ReSe<sub>2</sub>, the Raman scattering response for linearly polarized excitation (532 nm laser with *x*-direction

polarization) was examined. The measurements were performed by varying the polarization direction ( $\theta$ ) of the incident laser from 0° to 360° with 10° steps. Figure 4(a) depicts the evolution of the Raman spectrum with respect to  $\theta$ . Here, we observe that the peak intensity of each Raman mode varied significantly with a period of 180°, and the peak positions remained unchanged. This dependence is clearly observed in the polar plots (Fig. 4(b)) and the 2D mapping (Fig. 4(c)) of the peak intensity with respect to the rotation angle of the laser polarization direction. The intensity of the Raman mode of ReSe<sub>2</sub> under polarized incident light is theoretically calculated as follows

$$I \propto |a \cos \theta + d \sin \theta|^2 + |d \cos \theta + b \sin \theta|^2 \quad (3)$$

where *a*, *b*, and *d* are the values determined by the vibration of each Raman mode [10]. Figure 4(b) shows the plots of the peaks at 125, 160, and 174 cm<sup>-1</sup>, which well match the calculation results. Because modifying the relative angle between the laser polarization direction and the crystal orientation results in the variation of the Raman intensities, we

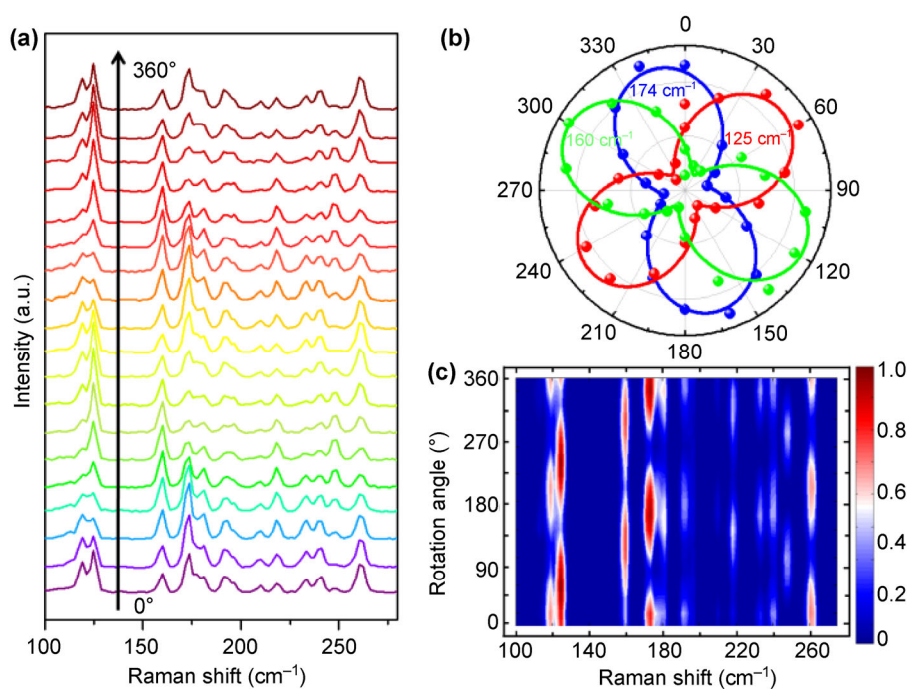


**Figure 4** Angle-dependent polarized Raman spectra of the grown ReSe<sub>2</sub>. (a) Polarized Raman spectra with respect to the rotation angle ( $\theta$ ) of the laser polarization direction. (b) Polar plots for the ReSe<sub>2</sub> modes corresponding to peak intensities of 125 cm<sup>-1</sup> (red line), 160 cm<sup>-1</sup> (green line), and 174 cm<sup>-1</sup> (blue line) with respect to  $\theta$ . (c) 2D mapping of the Raman spectra with respect to the rotation angle  $\theta$  (intensity is normalized with respect to the strongest peak at 125 cm<sup>-1</sup>).



can utilize polarization-resolved Raman measurements to identify the crystal orientation of the CVD-grown ReSe<sub>2</sub>.

Transport measurements were performed to characterize the electrical and photoelectric properties of our CVD-grown ReSe<sub>2</sub> film. Figure 5(a) shows a schematic of an FET device made from the ReSe<sub>2</sub> film. The linear source-drain current–voltage ( $I_{ds}$ – $V_{ds}$ ) characteristic suggests that Ohmic contacts were formed between the Cr/Au metal pads and ReSe<sub>2</sub> (Fig. 5(b)). The ReSe<sub>2</sub> device exhibited p-type conduction with a current ON/OFF ratio up to 10<sup>5</sup> and a threshold voltage of –10 V (Fig. 5(c)). According to the equation for the carrier mobility

$$\mu = \frac{L}{WV_{ds}C_g} \cdot \frac{dI_{ds}}{dV_g} \quad (4)$$

where  $L$ ,  $W$ ,  $C_g$ , and  $V_g$  represent the channel length, channel width, gate capacitance per unit area, and gate voltage, respectively; the field-effect hole mobility of this ReSe<sub>2</sub> FET was calculated to be 0.98 cm<sup>2</sup>/(V·s).

The mobility of the CVD-grown ReSe<sub>2</sub> was lower than that of the exfoliated samples (9.78 cm<sup>2</sup>/(V·s)) but exhibited great improvement over that of a recently reported CVD-grown sample (1.36 × 10<sup>-3</sup> cm<sup>2</sup>/(V·s)) [27]. Importantly, early reports of CVD-grown ReSe<sub>2</sub> and MoS<sub>2</sub> also indicated relatively low mobilities, but the mobility increased with further study and optimization of the growth conditions. The grain boundary between the sub-domains of ReSe<sub>2</sub> may be one reason for the mobility decrease and can be improved via the controlled growth of single-crystal ReSe<sub>2</sub>. Furthermore, the ReSe<sub>2</sub> device exhibited an outstanding photoresponse to NIR light (Fig. 5(d)), with responsivity up to 8.4 and 5.1 A/W for 850 and 940 nm light, respectively. It had a fast photoresponse, with photocurrent rise and decay stage times up to the millisecond level (Fig. S6 in the ESM). These results are comparable to those of mechanically exfoliated ReSe<sub>2</sub> flakes (responsivity: 55.5 A/W at 633 nm), indicating the high crystal quality of our grown material [16, 39]. The p-type conduction and narrow bandgap of ReSe<sub>2</sub>, which are rare in most TMDs,

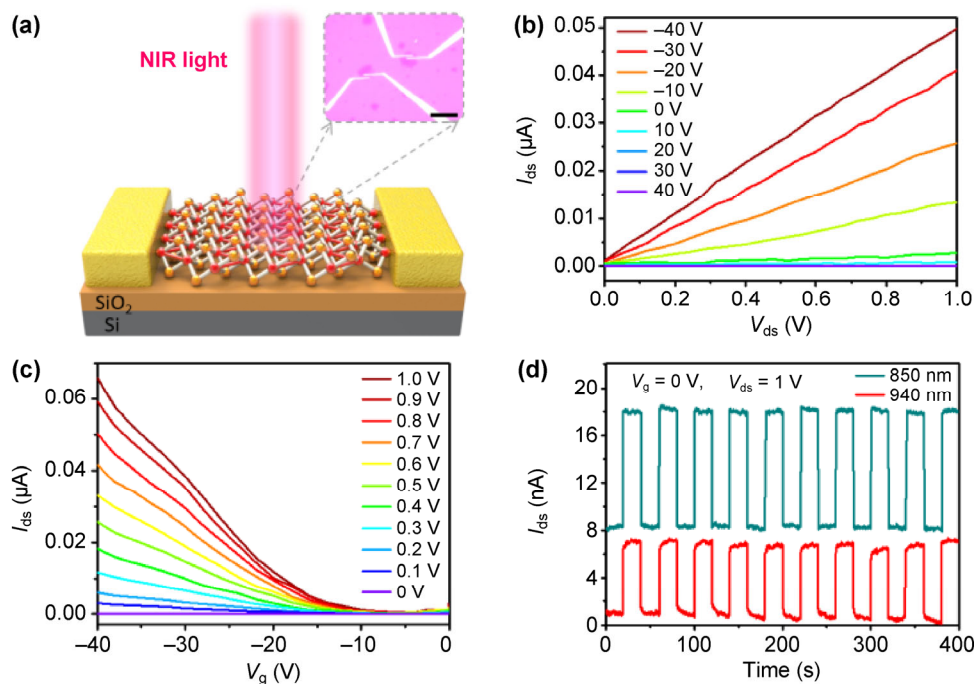


**Figure 5** Electrical and photoelectrical properties of the device made from the CVD-grown ReSe<sub>2</sub> sample. (a) Typical OM image of the ReSe<sub>2</sub> device on a 300-nm SiO<sub>2</sub>/Si substrate. The scale bar represents 20 μm. (b)  $I_{ds}$  vs.  $V_{ds}$  characteristics of our ReSe<sub>2</sub> FET device at various gate voltages. (c)  $I_{ds}$  vs.  $V_g$  curve for the same device at various values of  $V_{ds}$ . (d)  $I_{ds}$  vs. time when the device was illuminated with 850- and 940-nm light at an irradiance of 6.07 and 6.97 mW/cm<sup>2</sup>, respectively. The measurement was performed at a constant  $V_{ds}$  (1 V) in ambient air, with a working device area of 19 μm<sup>2</sup>.

endow it with great potential for application in future electronic and optoelectronic devices.

### 3 Conclusions

A large-area and highly crystalline ReSe<sub>2</sub> film with a uniform monolayer thickness was synthesized on mica substrates by van der Waals epitaxy. The constructed micro-reactor, which plays a space-confinement role to reduce the nucleation density and the growth rate of ReSe<sub>2</sub>, is critical for the controlled growth of ReSe<sub>2</sub> with the volatile ReO<sub>3</sub> as Re precursor. The out-of-plane growth and anisotropic growth of ReSe<sub>2</sub>, which are serious problems in the preparation of low-lattice symmetry 2D materials, were suppressed by growing it on a low-surface energy substrate (mica) at a low temperature (450–700 °C). The angle-dependent polarized Raman spectra of the grown ReSe<sub>2</sub> confirmed its strong anisotropy. Moreover, the electrical and photoelectric properties of the grown ReSe<sub>2</sub> were comparable to those of mechanically exfoliated ReSe<sub>2</sub> flakes. Our research not only promotes the large-scale application of ReSe<sub>2</sub> in high-performance electronic devices but also clarifies the synthesis mechanism of low-lattice symmetry 2D materials.

## 4 Experimental

### 4.1 Growth and transfer of ReSe<sub>2</sub> monolayer

The CVD growth was performed in a single temperature-zone tubular furnace at the atmospheric pressure. Before the growth, ReO<sub>3</sub> powder (purity of 99.9%) and Se powder (purity of 99.99%) were placed at the center and the outside edge (~300 °C) of the hot zone, respectively. Two (or several) pieces of freshly cleaved fluorophlogopite mica substrate (1 cm<sup>2</sup> in size) were stacked to form a micro-reactor, simply by placing one piece onto another. The electrostatic force between the two mica substrates caused them to adsorb together tightly. Then, the micro-reactor (stacked mica substrates) was placed onto a ceramic boat containing ReO<sub>3</sub> in the hot center of the tube furnace (Fig. 1(a)). A mixture of Ar (80 sccm) and H<sub>2</sub> (1–10 sccm) was used as the carrier gas during the whole growth process. The furnace temperature was increased

to the growth temperature (450–700 °C) at a rate of 25 °C/min and then maintained for 3–10 min for the ReSe<sub>2</sub> growth. The as-grown ReSe<sub>2</sub> film was transferred onto a SiO<sub>2</sub>/Si (300 nm) substrate via the PMMA-mediated transfer method. A hydrofluoric acid (20 wt.%) solution was used as the etchant to exfoliate the ReSe<sub>2</sub> film from the mica substrate.

### 4.2 Characterizations of epitaxial monolayer ReSe<sub>2</sub>

The morphology and structure of the ReSe<sub>2</sub> film were examined using OM (Olympus BX51), AFM (Bruker Dimension ICON), Raman spectroscopy (Renishaw), and field-emission TEM (Tecnai G2 F20). A lacey C film supported on Cu grids was used for the TEM characterization, onto which the ReSe<sub>2</sub> layer was transferred via a method similar to that described in the previous paragraph. The composition of the ReSe<sub>2</sub> sample was confirmed by XPS (Kratos Analytical). The fluorescence spectra were measured using a homemade spectrometer. For angle-resolved polarized Raman measurements, a polarization analyzer was placed in the path of the incident laser to obtain the *x*-direction polarized light, and the polarized Raman spectra were obtained by rotating the laser polarization direction using a half-wave plate.

### 4.3 Device fabrication and electrical measurement

The monolayer ReSe<sub>2</sub> film was transferred onto a SiO<sub>2</sub>/Si (300 nm) substrate. The device was fabricated using standard electron-beam lithography and liftoff procedures. Electrical contacts with the ReSe<sub>2</sub> sample were formed by the thermal evaporation of 5 nm of Cr and 50 nm of Au. The electrical and photoelectrical properties were measured using an Agilent B2912A source-meter unit in ambient air. Light-emitting diodes with wavelengths of 850 and 940 nm were used as the light source in the photoelectric measurements of the ReSe<sub>2</sub> device.

## Acknowledgements

The authors acknowledge the insightful suggestions and comments from Dr. S. C. Zhang and N. N. Mao at Peking University. This work was supported by the National Natural Science Foundation of China (Nos.

51502167 and 21473110), and the fundamental Research Funds for the Central Universities (No. GK201502003), L. Z. and J. K. acknowledge the funding by the Center for Integrated Quantum Materials under NSF (No. DMR-1231319).

**Electronic Supplementary Material:** Supplementary material (thermogravimetric analysis of  $\text{ReO}_3$ , scalable growth of large-area  $\text{ReSe}_2$  film by using space-confined CVD growth, substrate dependent growth behavior of  $\text{ReSe}_2$ , effect of hydrogen concentration on the  $\text{ReSe}_2$  growth, Raman spectrum of  $\text{ReSe}_2$  grown at different temperature, and photoresponse dynamic of  $\text{ReSe}_2$  photodetector) is available in the online version of this article at <http://dx.doi.org/10.1007/s12274-017-1477-7>.

## References

- [1] Tongay, S.; Sahin, H.; Ko, C.; Luce, A.; Fan, W.; Liu, K.; Zhou, J.; Huang, Y. S.; Ho, C. H.; Yan, J. Y. et al. Monolayer behaviour in bulk  $\text{ReS}_2$  due to electronic and vibrational decoupling. *Nat. Commun.* **2014**, *5*, 3252.
- [2] Lorchat, E.; Froehlicher, G.; Berciaud, S. Splitting of interlayer shear modes and photon energy dependent anisotropic Raman response in  $N$ -layer  $\text{ReSe}_2$  and  $\text{ReS}_2$ . *ACS Nano* **2016**, *10*, 2752–2760.
- [3] Hart, L.; Dale, S.; Hoye, S.; Webb, J. L.; Wolverson, D. Rhenium dichalcogenides: Layered semiconductors with two vertical orientations. *Nano Lett.* **2016**, *16*, 1381–1386.
- [4] Hafeez, M.; Gan, L.; Li, H. Q.; Ma, Y.; Zhai, T. Y. Large-area bilayer  $\text{ReS}_2$  film/multilayer  $\text{ReS}_2$  flakes synthesized by chemical vapor deposition for high performance photodetectors. *Adv. Funct. Mater.* **2016**, *26*, 4551–4560.
- [5] Yang, S. X.; Wang, C.; Sahin, H.; Chen, H.; Li, Y.; Li, S. S.; Suslu, A.; Peeters, F. M.; Liu, Q.; Li, J. B. et al. Tuning the optical, magnetic, and electrical properties of  $\text{ReSe}_2$  by nanoscale strain engineering. *Nano Lett.* **2015**, *15*, 1660–1666.
- [6] Zhong, H. X.; Gao, S. Y.; Shi, J. J.; Yang, L. Quasiparticle band gaps, excitonic effects, and anisotropic optical properties of the monolayer distorted 1T diamond-chain structures  $\text{ReS}_2$  and  $\text{ReSe}_2$ . *Phys. Rev. B* **2015**, *92*, 115438.
- [7] Lin, Y. C.; Komsa, H. P.; Yeh, C. H.; Björkman, T.; Liang, Z. Y.; Ho, C. H.; Huang, Y. S.; Chiu, P. W.; Krasheninnikov, A. V.; Suenaga, K. Single-layer  $\text{ReS}_2$ : Two-dimensional semiconductor with tunable in-plane anisotropy. *ACS Nano* **2015**, *9*, 11249–11257.
- [8] Chenet, D. A.; Aslan, O. B.; Huang, P. Y.; Fan, C.; van der Zande, A. M.; Heinz, T. F.; Hone, J. C. In-plane anisotropy in mono- and few-layer  $\text{ReS}_2$  probed by Raman spectroscopy and scanning transmission electron microscopy. *Nano Lett.* **2015**, *15*, 5667–5672.
- [9] Liu, E. F.; Fu, Y. J.; Wang, Y. J.; Feng, Y. Q.; Liu, H. M.; Wan, X. G.; Zhou, W.; Wang, B. G.; Shao, L. B.; Ho, C. H. et al. Integrated digital inverters based on two-dimensional anisotropic  $\text{ReS}_2$  field-effect transistors. *Nat. Commun.* **2015**, *6*, 6991.
- [10] Zhao, H.; Wu, J. B.; Zhong, H. X.; Guo, Q. S.; Wang, X. M.; Xia, F. N.; Yang, L.; Tan, P. H.; Wang, H. Interlayer interactions in anisotropic atomically thin rhenium diselenide. *Nano Res.* **2015**, *8*, 3651–3661.
- [11] Zhang, L. M.; Liu, K. H.; Wong, A. B.; Kim, J.; Hong, X. P.; Liu, C.; Cao, T.; Louie, S. G.; Wang, F.; Yang, P. D. Three-dimensional spirals of atomic layered  $\text{MoS}_2$ . *Nano Lett.* **2014**, *14*, 6418–6423.
- [12] Wu, J. X.; Mao, N. N.; Xie, L. M.; Xu, H.; Zhang, J. Identifying the crystalline orientation of black phosphorus using angle-resolved polarized Raman spectroscopy. *Angew. Chem., Int. Ed.* **2015**, *54*, 2366–2369.
- [13] Wang, X. M.; Jones, A. M.; Seyler, K. L.; Tran, V.; Jia, Y. C.; Zhao, H.; Wang, H.; Yang, L.; Xu, X. D.; Xia, F. N. Highly anisotropic and robust excitons in monolayer black phosphorus. *Nat. Nano* **2015**, *10*, 517–521.
- [14] Corbet, C. M.; McClellan, C.; Rai, A.; Sonde, S. S.; Tutuc, E.; Banerjee, S. K. Field effect transistors with current saturation and voltage gain in ultrathin  $\text{ReS}_2$ . *ACS Nano* **2015**, *9*, 363–370.
- [15] Liu, F. C.; Zheng, S. J.; He, X. X.; Chaturvedi, A.; He, J. F.; Chow, W. L.; Mion, T. R.; Wang, X. L.; Zhou, J. D.; Fu, Q. D. et al. Highly sensitive detection of polarized light using anisotropic 2D  $\text{ReS}_2$ . *Adv. Funct. Mater.* **2016**, *26*, 1169–1177.
- [16] Yang, S. X.; Tongay, S.; Yue, Q.; Li, Y. T.; Li, B.; Lu, F. Y. High-performance few-layer Mo-doped  $\text{ReSe}_2$  nanosheet photodetectors. *Sci. Rep.* **2014**, *4*, 5442.
- [17] Liu, E. F.; Long, M. S.; Zeng, J. W.; Luo, W.; Wang, Y. J.; Pan, Y. M.; Zhou, W.; Wang, B. G.; Hu, W. D.; Ni, Z. H. et al. High responsivity phototransistors based on few-layer  $\text{ReS}_2$  for weak signal detection. *Adv. Funct. Mater.* **2016**, *26*, 1938–1944.
- [18] Zhang, E. Z.; Jin, Y. B.; Yuan, X.; Wang, W. Y.; Zhang, C.; Tang, L.; Liu, S. S.; Zhou, P.; Hu, W. D.; Xiu, F. X.  $\text{ReS}_2$ -based field-effect transistors and photodetectors. *Adv. Funct. Mater.* **2015**, *25*, 4076–4082.
- [19] Wang, X. T.; Huang, L.; Peng, Y. T.; Huo, N. J.; Wu, K. D.; Xia, C. X.; Wei, Z. M.; Tongay, S.; Li, J. B. Enhanced rectification, transport property and photocurrent generation of multilayer  $\text{ReSe}_2/\text{MoS}_2$  p-n heterojunctions. *Nano Res.* **2016**, *9*, 507–516.

- [20] Liu, S. J.; Huang, L.; Wu, K. D.; Wei, Z. M.; Huang, B. J.; Meng, X. Q.; Tongay, S.; Liu, J.; Li, J. B.; Chen, H. D. Tuned polarity and enhanced optoelectronic performances of few-layer  $\text{Nb}_{0.125}\text{Re}_{0.875}\text{Se}_2$  flakes. *Appl. Phys. Lett.* **2016**, *109*, 112102.
- [21] Wolverson, D.; Crampin, S.; Kazemi, A. S.; Ilie, A.; Bending, S. J. Raman spectra of monolayer, few-layer, and bulk  $\text{ReSe}_2$ : An anisotropic layered semiconductor. *ACS Nano* **2014**, *8*, 11154–11164.
- [22] Lv, R. T.; Robinson, J. A.; Schaak, R. E.; Sun, D.; Sun, Y. F.; Mallouk, T. E.; Terrones, M. Transition metal dichalcogenides and beyond: Synthesis, properties, and applications of single- and few-layer nanosheets. *Acc. Chem. Res.* **2015**, *48*, 56–64.
- [23] Li, H.; Cao, J.; Zheng, W. S.; Chen, Y. L.; Wu, D.; Dang, W. H.; Wang, K.; Peng, H. L.; Liu, Z. F. Controlled synthesis of topological insulator nanoplate arrays on mica. *J. Am. Chem. Soc.* **2012**, *134*, 6132–6135.
- [24] Chen, W.; Zhao, J.; Zhang, J.; Gu, L.; Yang, Z. Z.; Li, X. M.; Yu, H.; Zhu, X. T.; Yang, R.; Shi, D. X. et al. Oxygen-assisted chemical vapor deposition growth of large single-crystal and high-quality monolayer  $\text{MoS}_2$ . *J. Am. Chem. Soc.* **2015**, *137*, 15632–15635.
- [25] He, X. X.; Liu, F. C.; Hu, P.; Fu, W.; Wang, X. L.; Zeng, Q. S.; Zhao, W.; Liu, Z. Chemical vapor deposition of high-quality and atomically layered  $\text{ReS}_2$ . *Small* **2015**, *11*, 5423–5429.
- [26] Gao, J.; Li, L.; Tan, J. W.; Sun, H.; Li, B. C.; Idrobo, J. C.; Singh, C. V.; Lu, T. M.; Koratkar, N. Vertically oriented arrays of  $\text{ReS}_2$  nanosheets for electrochemical energy storage and electrocatalysis. *Nano Lett.* **2016**, *16*, 3780–3787.
- [27] Hafeez, M.; Gan, L.; Li, H. Q.; Ma, Y.; Zhai, T. Y. Chemical vapor deposition synthesis of ultrathin hexagonal  $\text{ReSe}_2$  flakes for anisotropic raman property and optoelectronic application. *Adv. Mater.* **2016**, *28*, 8296–8301.
- [28] Keyshar, K.; Gong, Y. J.; Ye, G. L.; Brunetto, G.; Zhou, W.; Cole, D. P.; Hackenberg, K.; He, Y. M.; Machado, L.; Kabbani, M. et al. Chemical vapor deposition of monolayer rhenium disulfide ( $\text{ReS}_2$ ). *Adv. Mater.* **2015**, *27*, 4640–4648.
- [29] Wang, Q. S.; Xu, K.; Wang, Z. X.; Wang, F.; Huang, Y.; Safdar, M.; Zhan, X. Y.; Wang, F. M.; Cheng, Z. Z.; He, J. Van der waals epitaxial ultrathin two-dimensional nonlayered semiconductor for highly efficient flexible optoelectronic devices. *Nano Lett.* **2015**, *15*, 1183–1189.
- [30] Jiang, Y.; Zhang, X.; Wang, Y.; Wang, N.; West, D.; Zhang, S. B.; Zhang, Z. Vertical/planar growth and surface orientation of  $\text{Bi}_2\text{Te}_3$  and  $\text{Bi}_2\text{Se}_3$  topological insulator nanoplates. *Nano Lett.* **2015**, *15*, 3147–3152.
- [31] Zhang, E. Z.; Wang, P.; Li, Z.; Wang, H. F.; Song, C. Y.; Huang, C.; Chen, Z. G.; Yang, L.; Zhang, K. T.; Lu, S. H. et al. Tunable ambipolar polarization-sensitive photodetectors based on high-anisotropy  $\text{ReSe}_2$  nanosheets. *ACS Nano* **2016**, *10*, 8067–8077.
- [32] Splendiani, A.; Sun, L.; Zhang, Y. B.; Li, T. S.; Kim, J.; Chim, C. Y.; Galli, G.; Wang, F. Emerging photoluminescence in monolayer  $\text{MoS}_2$ . *Nano Lett.* **2010**, *10*, 1271–1275.
- [33] Chang, Y. H.; Zhang, W. J.; Zhu, Y. H.; Han, Y.; Pu, J.; Chang, J. K.; Hsu, W. T.; Huang, J. K.; Hsu, C. L.; Chiu, M. H. et al. Monolayer  $\text{MoSe}_2$  grown by chemical vapor deposition for fast photodetection. *ACS Nano* **2014**, *8*, 8582–8590.
- [34] Mitioglu, A. A.; Galkowski, K.; Surrente, A.; Klopotoski, L.; Dumcenco, D.; Kis, A.; Maude, D. K.; Plochocka, P. Magnetoexcitons in large area CVD-grown monolayer  $\text{MoS}_2$  and  $\text{MoSe}_2$  on sapphire. *Phys. Rev. B.* **2016**, *93*, 165412.
- [35] Lu, X.; Utama, M. I. B.; Lin, J. H.; Gong, X.; Zhang, J.; Zhao, Y. Y.; Pantelides, S. T.; Wang, J. X.; Dong, Z. L.; Liu, Z. et al. Large-area synthesis of monolayer and few-layer  $\text{MoSe}_2$  films on  $\text{SiO}_2$  substrates. *Nano Lett.* **2014**, *14*, 2419–2425.
- [36] Wang, X. L.; Gong, Y. J.; Shi, G.; Chow, W. L.; Keyshar, K.; Ye, G. L.; Vajtai, R.; Lou, J.; Liu, Z.; Ringe, E. et al. Chemical vapor deposition growth of crystalline monolayer  $\text{MoSe}_2$ . *ACS Nano* **2014**, *8*, 5125–5131.
- [37] Cui, F. F.; Wang, C.; Li, X. B.; Wang, G.; Liu, K. Q.; Yang, Z.; Feng, Q. L.; Liang, X.; Zhang, Z. Y.; Liu, S. Z. et al. Tellurium-assisted epitaxial growth of large-area, highly crystalline  $\text{ReS}_2$  atomic layers on mica substrate. *Adv. Mater.* **2016**, *28*, 5019–5024.
- [38] Wu, K. D.; Chen, B.; Yang, S. J.; Wang, G.; Kong, W.; Cai, H.; Aoki, T.; Soignard, E.; Marie, X.; Yano, A. et al. Domain architectures and grain boundaries in chemical vapor deposited highly anisotropic  $\text{ReS}_2$  monolayer films. *Nano Lett.* **2016**, *16*, 5888–5894.
- [39] Yang, S. X.; Tongay, S.; Li, Y.; Yue, Q.; Xia, J. B. S.; Li, S.; Li, J. B.; Wei, S. H. Layer-dependent electrical and optoelectronic responses of  $\text{ReSe}_2$  nanosheet transistors. *Nanoscale* **2014**, *6*, 7226–7231.